Tracking submarine volcanic activity at Monowai: Constraints from long-range hydroacoustic measurements

Authors: D. Metz[1*], A. B. Watts[1], I. Grevemeyer[2], M. Rodgers[3]

[1]Department of Earth Sciences, South Parks Road, Oxford OX1 3AN, United Kingdom

[2]GEOMAR Helmholtz Centre for Ocean Research Kiel, Kiel, Germany

[3]School of Geosciences, University of South Florida, Tampa, Florida, USA

* Now at: Research and Development Center for Earthquake and Tsunami, Japan Agency for Marine-Earth Science and Technology (JAMSTEC), Yokohama, Kanagawa, Japan

Corresponding Author: Dirk Metz (dirk.metz@earth.ox.ac.uk)

Highlights

- Volcanic activity at Monowai is detected by an IMS hydrophone array at Juan Fernández Islands, Southeast Pacific Ocean
- 82 discrete episodes of activity have been identified in a 3.5-year record
- Monowai is one of the most active submarine arc volcanoes currently known

Index Terms: Monowai, submarine volcanism, hydroacoustics, Pacific Ocean, IMS, CTBTO

Abstract

Monowai is a submarine volcanic center in the Kermadec Arc, Southwest Pacific Ocean. In the past, activity at the volcano had been intermittently observed in the form of fallout at the sea surface, discolored water, changes in seafloor topography, and T phase seismicity, but there is no continuous record for more recent years. In this study, we investigated 3.5 years of recordings at a hydrophone array of the International Monitoring System (IMS), located near Juan Fernández Islands for long-range underwater sound waves from Monowai. Results from direction-of-arrival calculations and density-based spatial clustering indicate that 82 discrete episodes of activity occurred between July 2003 and March 2004, and from April 2014 to January 2017. Volcanic episodes are typically spaced days to weeks apart, range from hours to days in length, and amount to a cumulative sum of 137 days of arrivals in total, making Monowai one of the most active submarine arc volcanoes on Earth. The resolution of the hydrophone recordings surpasses broadband network data by at least one order of magnitude, identifying seismic events as low as 2.2 m_b in the Kermadec Arc region. Further observations suggest volcanic activity at a location approximately 400 km north of Monowai in the Tonga Arc, and at Healy or Brothers volcano in the southern Kermadec Arc. Our findings are consistent with previous studies and highlight the exceptional capabilities of the IMS network for the scientific study of active volcanism in the global ocean.

1. Introduction

Little is known about the rates of submarine arc volcanism. Continuous surveys of known volcanoes are hindered by their remoteness and the inherent inaccessibility of the ocean environment for conventional monitoring techniques, for example satellite altimetry, thermal imaging, or measuring atmospheric gas fluxes (e.g., Calkins et al., 2008; Mather et al., 2012). Hence, the location and timing of eruptions remain poorly constrained, and few active sites along submarine arcs have been studied over longer timescales (Embley et al., 2006; Schnur et al., 2017). Here, we attempt to overcome these observational limitations by using long-range underwater sound waves to study volcanic activity at Monowai, a submarine volcano in the Tonga-Kermadec Arc.

Located at 25.89°S, 177.18°W in the northern Kermadec Arc, Southwest Pacific Ocean, Monowai is a known example of on-going submarine volcanic activity. The edifice consists of an active stratovolcanic cone, rising from approximately 1200 to 100 m below sea level, and a flanking caldera of approximately 10 km in diameter (Wormald et al., 2012; Paulatto et al., 2014). There is a diverse record of activity at Monowai, including direct observations of discolored surface water, gas emissions, and pumice rafts (Davey, 1980). In one instance, activity was inferred from changes in sea surface chlorophyll and particulate matter content, as nutrient-rich fallout from the volcano had significantly increased local phytoplankton concentration (O'Malley et al., 2014). Further observations include onsite recordings of acoustic shockwaves (Werner et al., 2013) as well as hour to day-long swarms of T phases registered by seismometers in the Southwest Pacific region (Talandier and Okal, 1987). Swath bathymetric mapping has revealed the dynamic topography of the stratocone, which

has undergone repeated phases of growth and collapse, thus leading to changes in seafloor depth on the order of tens of meters over the past two decades (Wright et al., 2008; Chadwick et al., 2008a). During the most recent documented eruption in May 2011, a five days long burst of T phases, recorded at broadband seismometers at Rarotonga (Cook Islands), Papeete (Tahiti) and Nuku Hiva (Marquesas Islands), could be linked to the growth of a 72 m summit cone and a flanking sector collapse of 18 m (Watts et al., 2012). Furthermore, long-range underwater sound waves associated with the same volcanic episode have been remotely detected by a hydrophone array near Ascension Island in the southern Equatorial Atlantic Ocean, over a geodesic range of 15,800 km (Metz et al., 2016). Activity at Monowai may have occurred as recently as October 2014 and May 2016, when seismic amplitudes at Rarotonga station rose for multiple days and discolored water was reported during flyovers conducted by the Royal New Zealand Air Force (Global Volcanism Program, 2017).

Low-frequency underwater sound travels in the Sound Fixing and Ranging (SOFAR) channel, a distinct layer of minimum acoustic velocity in the oceanic water column (Tolstoy et al., 1949; Ewing et al., 1951). Earthquakes along active plate boundaries, i.e. mid-ocean ridges and subduction zones, are frequent sources of underwater sound signals that can be detected over hundreds to thousands of kilometers (Smith et al., 2002; Graeber and Piserchia, 2004). Hydroacoustic observations also include recordings of volcanic activity, in particular along the submarine arcs of the western Pacific region, for example at Fukutoku-Okanoba in the Volcano Islands (Dziak and Fox, 2002), South Sarigan in the Mariana Arc (Green et al., 2013), or Hunga Ha'apai-Hunga Tonga volcano in the Tonga-Kermadec Arc (Bohnenstiehl et al., 2013). Acoustic phases can be converted effectively during the transition from ocean to land, thus becoming detectable by both hydrophones and land-based seismometers (Stevens et al., 2001). Due to the efficient propagation of low-frequency underwater sound even over

megameter distances, such seismoacoustic arrivals, also known as seismic tertiary waves or 'T phases', can be used to improve earthquake detection and relocation, especially where monitoring by conventional methods is not feasible (Helffrich et al., 2006).

Long-range propagation of low-frequency underwater sound phases is a key feature of the hydroacoustic waveform component of the International Monitoring System (IMS). As part of the verification regime for the Comprehensive Nuclear-Test-Ban Treaty (CTBT) of 1996, the objective of the IMS hydrophone network is to globally detect underwater nuclear explosions, but the comprehensive installation also enables the study of natural phenomena, including, amongst others, earthquake rupture propagation (Guilbert et al., 2005; Tolstoy and Bohnenstiehl, 2005), tsunami signals (Matsumoto et al., 2016), ocean acoustic propagation (Evers and Snellen, 2015), and marine mammal vocalization (Le Bras et al., 2016; Ward et al., 2017). A total of eleven hydroacoustic receiver sites are in operation worldwide, six of which are hydrophone triplet arrays, typically deployed at remote ocean islands and near the SOFAR channel axis. Here, we focus on recordings from IMS station H03 at Juan Fernández Islands, located approximately 700 km off the coast of Chile, where episodes of volcanic activity at Monowai can be detected from across the southern Pacific basin (Figure 1a).

2. Hydrophone Triplet Data and Processing

2.1 Data Availability and Instrumentation

Station H03 of the International Monitoring System consists of two bottom moored hydrophone arrays, located approximately 15 km north (H03N) and south (H03S) of Isla Robinson Crusoe, the easternmost island in the Juan Fernández archipelago (Figure 1b). The southern array was in operation from July 2003 to March 2004, when data transmission

ceased due to a cable failure. After the loss of the remaining installation in the tsunami following the 2010 Maule earthquake (Fritz et al., 2011), the array became fully operational again in April 2014, thus providing a record of approximately 3.5 years for the 2003-04 period and from April 2014 to January 2017. Since its first installation in 2003, H03S has exceeded its designated uptime of 97.5%, with only nine days of the entire record being omitted from our calculations due to missing or corrupted data. The three hydrophones, H03S1-3, are moored near the SOFAR channel axis at 830 m water depth (Supporting Figure S1), with elements organized in a tripartite configuration and at an equidistant spacing of 2 km (Figure 1c). Acoustic measurements are made at 250 Hz and transmitted in near-real time to the International Data Centre (IDC) in Vienna for routine processing and analyst review (Hanson et al., 2001).

We note that arrivals from Monowai show lower phase coherency at the northern array and appear attenuated by 4-8 dB compared to H03S. This may be due to bathymetric blockage and scattering of the incoming signal by one or more unnamed seamounts west of Isla Robinson Crusoe, where the seafloor shoals to depths of less than 150 m. As the east-west-trending archipelago effectively dissects the field of view of the two triplets, activity at Monowai cannot be reliably tracked at H03N by the methods outlined here. Furthermore, the Fijian islands as well as several seamounts in the Marshall Islands obstruct source-receiver paths to a second IMS hydrophone station located at Wake Island, Northwestern Pacific Ocean. Hence, we limit our study to the southern array of IMS station H03, Juan Fernández Islands.

2.2 Direction-of-Arrival Calculations and Detection

Hydrophone recordings are corrected for instrument response and the mean and trend is removed. Data is band-pass filtered between 4 and 12 Hz using a standard two-pole Butterworth filter. The cutoffs correspond to the frequencies at which long-range signals are detected most efficiently by IMS-type hydrophone arrays (Hanson and Bowman, 2006) and account for potential noise contamination from both ends of the spectrum, i.e. ocean microseism, marine mammal vocalization, and commercial shipping (e.g., Chapman and Price, 2011). As instruments are moored at similar water depths and potential sources are located in the acoustic far field, direction-of-arrival calculations follow a two-dimensional plane-wave fitting approach (Del Pezzo and Giudicepietro, 2002). Hydroacoustic recordings are subdivided into 1-min long, non-overlapping windows. Peak delay times t_{ij} between instrument pairs located at relative positions x_{ij} are derived from normalized cross-correlation of the windowed data. Subsequently, the slowness vector $p \equiv (p_x, p_y)$ of a planar wave front moving across the triplet array can be obtained by solving the following equation in a least-square sense:

$$t_{ij} = p \cdot \Delta x_{ij} \quad (1)$$

Apparent sound speed v across the array and angle of arrival θ, which represents the geodesic back azimuth between receiver and source along a great-circle path, are derived from

$$v = \left({p_x}^2 + {p_y}^2\right)^{-1/2} \quad (2)$$

and

$$\theta = \tan^{-1}\left(p_x / p_y\right). \quad (3)$$

Absolute errors for values calculated in (2) and (3) are obtained from the covariance matrix of the data and subsequent propagation of two sigma standard errors. Following a similar approach by Bohnenstiehl et al. (2013), peak delay times t_{ij}, t_{jk}, and t_{ki} between the three hydrophone pairs are summed to derive the closure function *cl* of the windowed cross-correlation. *cl* is assumed to approach zero for well-correlated signals and provides an additional quality constraint for filtering acoustic arrivals alongside the mean cross-correlation coefficient *cc* between the three hydrophone pairs:

$$cl = t_{ij} + t_{jk} + t_{ki} \quad (4)$$

A number of detection criteria are put in place to separate coherent acoustic phases from ambient noise. In order to eliminate arrivals not traveling in the SOFAR channel, signals not arriving within ± 50 m/s of 1481 m/s in a 1-min window are omitted from the data set, with 1481 m/s being the mean annual sound speed of the sound channel axis at Juan Fernández, estimated from data provided by the 2005 World Ocean Atlas (Supporting Figure S1). The minimum mean correlation coefficient between the hydrophone pairs is set to 0.3, which is consistent with empirically derived thresholds used by Nichols and Bradley (2016) and Li (2010) for IMS-type arrays of the same aperture and roughly corresponds to the noise floor for 1-min windows in the 4-12 Hz band (Metz et al., 2016). Following Graeber and Piserchia (2004) and Bohnenstiehl et al. (2014), the detection threshold of the closure function is set to |48| ms, corresponding to a maximum mismatch of 12 sampling intervals at 250 Hz.

2.3 Uncertainty analysis

We investigate the accuracy of returned back azimuth and sound speed values using air gun shots produced during the 2017 CEVICHE seismic reflection experiment during cruise MGL1701 of R/V Marcus G. Langseth (Rolling Deck to Repository Program, 2017). In January 2017, a seismic survey was carried out along the continental margin off-coast south central Chile and in the field of view of the H03S hydrophone array (Figure 2). As acoustic coupling into the deep sound channel is a function of seafloor slope, aspect, and depth near the signal source (Blackman et al., 2004; Bohnenstiehl et al., 2012), calibration data is limited to a subset of shots generated between 23:00 UTC 19 January and 05:00 UTC 21 January 2017 during survey line MC08R. During this time, the vessel passed through an area close to the continental shelf, where the seafloor topography is expected to be relatively even and the measured water depth varied by less than 200 m, thus enabling the constant deployment of homogeneous calibration shots at a source-receiver distance of 567 ± 7 km. As the incoming signal arrives at H03S from a southeastern direction, potential blockage due to the protruding bathymetry of the eastern Juan Fernández archipelago is avoided.

Applying the previously defined detection thresholds for sound speed, correlation coefficient, and closure function, a total of 1689 1-min detections are made at the H03S array. As the vessel moves along the survey line at a southwestern heading, back azimuths and sound speed distinctly stabilize between 109 and 129° and near 1480 m/s, respectively (Figure 2a-b). A comparison of the observed and the geodesic angles of arrival, the latter of which can be calculated from the logged position of the vessel along the survey line and respective shot times, shows that detections are accurate to within 0.2° and 0.4° at one and two standard deviation uncertainty (Figure 2c). We also observe a systematic error of -1.3±0.2°, which corresponds to an offset of 5-10 km abaft the vessel and, following Bohnenstiehl et al. (2012), suggests that coupling into the deep sound channel may take place in the form of

bottom-up reflection of acoustic energy at the seafloor. Derived sound speed values average at 1474 m/s and are well within two standard deviations (± 14 m/s) of the nominal estimate of 1481 m/s (Figure 2d). The offset could be explained by the movement of the hydrophone moorings due to deep ocean currents as well as local variations in ocean temperature, and hence, sound speed across the array (e.g., Evers and Snellen, 2015).

As acoustic recordings are binned to discrete intervals, individual shots are not identified. However, an estimate of data completeness can be made using the proportion of 1-min detections: Over a 30-hour period 4013 shots were deployed. Dividing this total by the average number of shots per minute (2.25) results in 1784 possible 1-min detections at H03S during the survey time. As 1689 1-min detections were made, we conclude that completeness is at least 95% within the defined detection thresholds. We also note that this proportion is not improved significantly by lowering one or all detection thresholds, which indicates that missing shots may have been misfired or blocked prior to their arrival at the H03S array, such that data completeness may in fact be even higher.

Excluding the systematic error, our calculations show that acoustic sources can be identified accurately to within 0.4° and 14 m/s (two sigma standard deviation) by the defined detection parameters. Measured uncertainties associated with derived back azimuths and slowness are consistent with values reported for IMS-type hydrophone deployments of the same configuration (Graeber and Piserchia, 2004; Hanson and Bowman, 2006).

3. Tracking volcanic activity at Monowai

3.1 Density-based clustering

Previous observations of distinct bursts of T phases, recorded by regional seismic stations, suggest that volcanic activity at Monowai typically occurs in episodes of hours to a few days in length (e.g., Chadwick et al., 2008a). In order to identify such discrete times of unrest in our data set, we exploit the fixed geometrical relationship between Monowai and the IMS hydrophone station. As arrivals associated with activity at the volcano move across the array and detection thresholds are applied, coherent phases stabilize along a distinct back azimuth over a short period of time, indicating a stationary, quasi-continuous source (Figure 3). A density-based spatial clustering algorithm, DBSCAN (Ester et al., 1996), can then be implemented to identify such densely-packed groups of detections, and hence detect and track potential episodes of volcanic activity in the data set. This approach is similar to a study of Averbuch et al. (2018), which relies on the Hough transform to identify low-level, persistent acoustic sources in the ambient noise field of an IMS infrasound array.

DBSCAN is based on the calculation of nearest neighbor distances and requires two input parameters: a minimum number of points m to form a cluster, and a search radius ε in the parameter space. The clustering process considers time and back azimuth of 1-min detections in a Cartesian plane and can be abstracted as follows: Data points with at least m points within a radius of ε are core points, which may either form a new cluster, or be assigned to a preexisting one if a core point already exists within ε distance. Data points reachable from a core point, but with less than m points in their ε neighborhood, are assigned to the cluster of the core point. All other data points are classified as noise. For this study, the minimum number of points m, i.e. 1-min detections, is set to 60, which corresponds to the shortest period of activity previously observed at Monowai, i.e. an hour-long eruptive collapse event in May 2002 (Wright et al., 2008). We define the search radius ε as 12 hours along the x-axis and 0.5° along the y-axis, which reflects the estimated accuracy of the plane wave fitting

routine and is twice the duration of the longest known intra-eruptive pause in activity at the volcano (Metz et al., 2016). As DBSCAN is computationally expensive and low-frequency arrivals from Monowai are not expected to vary by more than a few degrees (Bohnenstiehl et al., 2014), the spatial domain of the data set is limited to a ten degree range centered around the geodesic back azimuth to Monowai (243.8 ± 5°).

Given the above parameter settings, the shortest, most dense cluster identifiable by the DBSCAN algorithm would span 60 consecutive 1-min detections between 238.8 and 248.8° over the course of one hour along a constant back azimuth. Vice versa, the shortest, least dense cluster would hold 60 1-min detections along a constant back azimuth and be registered at over twice the length of the search radius, i.e. 24 hours. However, Figure 4a shows that due to the episodic nature of activity at Monowai (Chadwick et al., 2008a) and the low number of detections arriving from a similar direction, clustering results are extremely robust: Typically, hundreds to thousands of detections are made over short time scales and from a similar azimuth, which reduces the effect of the initial parameter setting. For example, relaxing m to 120 and ε to 1° and 24h, respectively, for the data shown in Figure 4a, results in the same number of clusters, with more than 99% of identical detections made.

3.2 Comparison of hydroacoustic and seismic recordings

Due to the large source-receiver distance between the volcano and the hydrophone array, some uncertainty exists as to whether clusters formed by the DBSCAN algorithm truly represent activity at Monowai, or whether they relate to other sources along the same great circle path, for example, swarms of tectonic earthquakes along the Chile and East Pacific Rise. However, direct relocation of T phase arrivals is not always possible, as seismic recordings at PPTF and TAOE station suffer from high ambient noise levels above 2 Hz. To

unambiguously identify Monowai as the signal source, we therefore resort to relative travel time differences between the broadband seismometer at Rarotonga and a single element of the H03S array (Metz et al., 2016).

For the time span of each cluster, envelope functions are calculated from normalized 1-min RMS amplitudes for the vertical component of the seismic station and hydrophone H03S1 (Figure 4b-c). In the case of Figure 4c, the two signals appear visually coherent, and cross-correlating their envelopes reveals a high degree of correlation at a peak delay time of 82 min (green line in Figure 4d), implying an average propagation speed of 1487 m/s. Considering the shift induced by the binning of the envelope functions to the full minute, a necessary prerequisite to derive meaningful correlation coefficients between the two time series, this is in agreement with the nominal arrival time offset between RAR and H03S1, which is estimated at 82 min 24 ± 14 sec, assuming a source at Monowai and a presumed average propagation speed of 1480 ± 5 m/s along the SOFAR channel axis (Munk and Forbes, 1989, see Figure 1a for source-receiver paths). We account for possible noise contamination of the derived envelopes, for example due to nearby ship traffic, seismic surveying, and earthquakes along the Tonga-Kermadec Arc or the Chilean subduction zone, by limiting the cross-correlation to the 6-hour segment of a cluster during which the highest number of 1-min detections are made (see grey shaded area in Figure 4c). Only if the maximum correlation coefficient peaks at the designated delay time of 82 min exactly, a cluster is added to the long-term record of activity at Monowai. For instance, the brown cluster in Figure 4a corresponds to a shallow (< 20 km hypocenter depth) 6.9 m_b magnitude earthquake (IRIS ID No. 4722859), and its subsequent aftershock sequence, that occurred on 23 June 2014 approximately 500 km south of the volcano in the central Kermadec Arc. The peak delay time of 78 min (brown line in Figure 4d) is in agreement with the catalogued epicenter

location at 30.0°S, 177.53°W, but fails to match the designated lag of 82 min, and hence is not added to the long-term record of activity. This validation process is repeated for all clusters formed by the DBSCAN algorithm (see also Supporting Figure S3).

4. Results

4.1 Volcanic activity at Monowai, 2003-2004 and 2014-2017

Following the approach outlined in the previous sections, a total of 82 clusters, consisting of 196,949 1-min detections over the course of 3.5 years, were identified and tracked back to Monowai, thus providing discrete times of activity at the volcano in the record of the H03S array between July 2003 and March 2004, and from April 2014 to January 2017 (Figure 5a-b). Remarkably, more than 98% of all detections within the processing window of 243.8 ± 5° are associated with activity at Monowai, suggesting that the volcano is the predominant source of low-frequency sound in the central Tonga-Kermadec Arc region.

Individual volcanic episodes last from a few hours to a maximum of 14 days and typically occur days to weeks apart, yet rarely exceeding more than one month of acoustic quiescence. Arrival rates can exceed 1320 1-min detections (i.e. a cumulative sum of 22 hours) per day and average at 725 across all episodes, indicating that, overall, acoustic phases from Monowai are registered every two minutes at the hydrophone array during times of volcanic activity (Figure 5 c-d). Notably, the longest pause in activity follows an intense series of four episodes in October and November 2014 that account for more than 20% of all registered detections and sustain some of the highest arrival rates in the data set (Figure 5e-f). Eruptive activity at Monowai during this time had also been noticed in the form of pumice rafts near the location of the volcano in late October 2014 (Global Volcanism Program, 2017), which

confirms our hydroacoustic observations and the results of the clustering algorithm. On a second occasion (Global Volcanism Program, 2017), reports of discolored surface water near Monowai coincide to the day with a cluster of detections in May 2016.

Mean RMS amplitudes per episode range from 88 dB to 110 dB re 1 µPa in the 4-12 Hz band, thus for most episodes exceeding background noise levels (~90 dB re 1 µPa, cf. Figure 3b) by up to 20 dB (Figure 5g-h). We observe maximum values of up to 128 dB for individual detections, which is on the same order as long-range acoustic measurements of the May 2011 eruption (Metz et al., 2016). Peak RMS amplitudes are typically scattered across individual episodes. This is distinctly different from the acoustic signature of tectonic earthquakes that normally exhibit an initial ramp-up of energy, corresponding to the arrival of the main shock, followed by swarms of weaker signals consisting of aftershocks and reflected sound waves (e.g., Hanson and Bowman, 2006). Although a detailed analysis of the frequency domain is beyond the scope of this study, we find a distinct absence of narrowband, harmonic tremor throughout the data set, which is different from other active sites in the Tonga-Kermadec Arc, e.g. Brothers or West Mata (Dziak et al., 2008; Bohnenstiehl et al., 2014). Instead, activity at Monowai consists of coherent, seconds to minute-long arrivals in the 4-20 Hz band, with occasional broadband bursts of up to 80 Hz and more, most likely representing an ensemble of signals generated by different processes, including volcano-tectonic earthquakes, fluid-driven oscillation, brittle fracturing, explosive fragmentation, and mass wasting events at the seafloor-ocean interface (Caplan-Auerbach et al., 2017, see also Figure 3a).

We further investigate whether activity at Monowai differs between the two subsets of volcanic episodes in 2003-04 and 2014-17. Results from a two-sample Kolmogorov-

Smirnov-Test (Massey, 1951) suggest that clustered detections from the two periods come from the same continuous distribution (5% significance level), indicating no significant change in the style of activity within the means of the tested statistical parameters, i.e. mean RMS acoustic magnitude in the 4-12 Hz band, episode duration, inter-episode time, and number of detections per day. We attribute the offset between mean back azimuths of volcanic episodes, averaging at 242.8 ± 0.3 and 243.4 ± 0.3° (two sigma standard deviation) for the 2003-04 and 2014-17 period, respectively, to the repositioning of the hydrophone sensors during the 2014 reinstallation of the H03 station. The systematic, counterclockwise deviation of 0.4 to 1° from the geodesic angle of arrival (243.8°) probably reflects a cumulative effect of uncertainty in sensor positioning (Nichols and Bradley, 2016), array geometry, and right-lateral refraction of the acoustic signal along its great circle path following horizontal temperature gradients in the southern Pacific Ocean as well as between the hydrophone elements (Munk et al., 1988; de Groot-Hedlin et al., 2009). Our estimates are in agreement with Evers et al. (2013) and Green et al. (2013), who place the error inherent to IMS-type triplet deployments at ≥ 0.4°.

In addition to volcanic episodes that can be traced back to Monowai, the DBSCAN algorithm identified a small number of other sources along the Tonga-Kermadec Arc. These clusters are usually associated with shallow (< 30 km focal depth), large magnitude tectonic earthquakes at locations distant from the volcano, and therefore produce different lag times during the cross-correlation procedure. For example, Figure 4a shows a cluster of 1-min detections of a catalogued 6.9 m_b event on 23 June 2014 in the central Kermadec Arc. The event produced numerous aftershocks in the range of 4.9 to 6.3 m_b over the following five days, thus explaining its detection by the clustering algorithm. In two cases, clusters neither match the back azimuth and delay time for a source at Monowai, nor the location and timing of a known

seismic event. These arrivals may be linked to volcanic activity at other locations in the central and southern Tonga-Kermadec Arc and are discussed in subsection 4.4 in more detail.

4.2 Relation to previous studies of T phase seismicity at Monowai

In a previous study, Chadwick et al. (2008a) investigated volcanic activity at Monowai between 1998 and 2007 from T phases recorded at TVO station, a broadband seismometer that is located at Taravao, Tahiti-Iti (Figure 1a), as part of the Polynesian Seismic Network (RSP, Talandier and Kuster, 1976). Although the T phase dataset overlaps with the 2003-2004 period of this study, comparison of the two records is not straightforward: Hydrophone data is binned to 1-min intervals and detection is based on signal coherence, whereas the broadband seismometer registered T phases represent discrete events defined by short-term/long-term filtering of energy ratios, and analyst review. Therefore, we focus here on timing and relative distribution rather than the absolute number of arrivals from the volcano.

Between July 2003 and March 2004, a total of 869 T phases were detected at the TVO seismometer and traced back to Monowai using further RSP stations for source location (Chadwick et al., 2008a). We find that 854 of these events, a relative share of 98.3%, fall within the bounds of one of the 16 episodes identified by density-based clustering of 49,838 hydroacoustic detections of the same time period (Figure 6). In all cases, 1-min detections precede the onset of T phase events registered at TVO by hours to days. For example, during the 8.5-days-long episode in February 2004, the first T phase event is registered more than five days after the first hydroacoustic arrival. During the same episode, T phase activity at TVO also ceases 18 hours prior to the last 1-min detection. On average, hydroacoustic detections are made 27 hours earlier, and outlast registered T phase events by 15 hours across all clusters of the 2003-2004 period. Furthermore, no T phases were observed during the

episodes in mid-November and mid-December 2003, both of which are within the bottom quarter of derived mean RMS acoustic magnitudes (98 and 92 dB re 1 µPa respectively, cf. Figure 5g).

Although differences in the timing of individual episodes exist, Figure 6 shows an excellent correlation (coefficient 0.98) between the normalized cumulative number of hydroacoustic detections at H03S and T phase events registered at the TVO station, indicating high similarity between the two time series. From this, we conclude that a) the relative distribution of arrivals is comparable between both datasets, confirming results from density-based clustering, and b) volcanism at Monowai indeed occurs in discrete episodes, with little to no activity observed in between. We further note that the ratio of hydroacoustic arrivals to T phases varies between a factor of 18 to 800 across all episodes. This disparity cannot be explained solely by differences in data segmentation between the two studies, but is most likely due to a combined effect of signal attenuation during the ocean-land conversion process, high noise levels at the seismometer that inhibit the detection of weaker events, and bias introduced by the parameter setting for declaring a T phase event in the seismic record of the TVO station. Thus, our findings illustrate the advantage of the acoustically 'quiet' hydrophone array over the land-based seismometer in detecting volcanic activity at Monowai, despite being located 6200 km further away from the source.

4.3 Resolution and seismic magnitude estimation

RMS amplitudes of 1-min detections associated with volcanic activity at Monowai follow a right-skewed normal distribution (Figure 7a), indicating that only events above a certain threshold are fully detected at the H03S array. In an attempt analogous to the derivation of the magnitude of completeness in seismic catalogues, we calculate the acoustic resolution of

the data set according to the maximum curvature method by Wiemer and Wyss (2000). Here, the amplitude level above which all arrivals can be successfully identified is defined as the data bin with the highest number of detections and roughly corresponds to the maximum value of the first derivative of the cumulative distribution shown Figure 7b (Woessner and Wiemer, 2005), i.e. 97 dB re 1 µPa. We interpret the relatively gradual drop-off of detections below this threshold as a combined effect of data segmentation, which can lead to the splitting of arrivals across two or more 1-min windows, and low-level variations in background noise, for example due to ice-generated tremor at southern latitudes (cf. Talandier et al., 2006), earthquake swarms, and commercial shipping (Sirovic et al., 2013). It is therefore reasonable to assume that activity at Monowai extends to levels below the detection threshold of the H03S array, and may occur even more frequently than observed in our analysis.

In a further step, hydrophone and seismometer recordings of tectonic earthquakes catalogued by the global IMS network are compared to estimate seismic magnitudes of activity at Monowai (Figure 7c). We account for attenuation of the signal in the solid earth and along the deep sound channel by constraining earthquake data to events with a catalogued depth of less than 80 km and a source-receiver distance similar to the geodesic path between the volcano and the H03S array, i.e. 8900 to 9200 km. Since Monowai itself is located within an aseismic 'gap' near the intersection of the Tonga-Kermadec Arc with the Louisville Ridge (Wyss et al., 1984; Bassett and Watts, 2015), only 28 earthquakes, scattered between 25 and 30°S along the northern Kermadec Arc to the south of the 'gap' (see inset of Figure 7c), fulfill the above criteria and were registered by the H03S1 hydrophone. At an average arrival length of 63 seconds and typically band pass-filtered between 4 and 12 Hz, the automated

parameter setting of the IMS processing stream closely matches the aggregate approach used in this study.

The equation of the least-square regression line shown in Figure 7c,

$$RMS\ Level\ (dB\ re\ 1\ \mu Pa) = 63.1 + 15.4 m_b, \quad (5)$$

indicates a linear relationship between acoustic and seismic measurements. The derived trend is significant (R^2 = 0.80) and in good agreement with observations by Pulli and Upton (2002) for the 2001 M_W 7.7 Bhuj earthquake sequence recorded at IMS hydrophones in the Indian Ocean. Acoustic resolution of 97 dB corresponds to a magnitude of completeness of 2.2 m_b which is an order of magnitude lower than the smallest tectonic event previously detected by IMS seismometers in the central Kermadec Arc region (3.3 m_b). Following this first order approximation, mean magnitudes of volcanic episodes at Monowai range from 1.6 (88 dB) to 3.1 m_b (110 dB) and are consistent with presumed levels of activity at the volcano during its 2011 eruption (~2 m_b, Metz et al., 2016). Since only a small number of individual arrivals reach peak amplitudes greater than 120 dB (> 3.5 m_b), overall levels of activity at the volcano most likely are too low to be resolved by a sparse network of land-based seismometers over teleseismic distances.

4.4 Further observations of volcanic activity in the Tonga-Kermadec Arc

As described in section 4.1, two clusters formed by the DBSCAN algorithm could not be linked to activity at Monowai or known seismic events along either the Tonga-Kermadec Arc or the East Pacific Rise, and therefore are investigated further.

The first cluster consists of 525 1-min detections received at the H03S array over the course of five days in December 2014. Acoustic phases arrive from a mean back azimuth of 246.4°, thus corresponding to a location in the southern Tonga Arc, approximately 400 km north of Monowai (Figure 8a-b). The activity is best described as a suite of short (< 5 sec), transient arrivals at frequencies below 16 Hz, rarely exceeding background noise levels by more than 10 dB in the 4-12 Hz processing band (Figure 8c-d). Known volcanically active sites in the area include Volcano 14, where hydrothermal venting was observed by Stoffers et al. (2006) during expedition SO167 aboard R/V *SONNE*, as well as a shallow seamount at 22.9°S, 176.4°W, also known as Pelorus or Pelorus Reef, that was previously identified as an acoustically and hydrothermally active source by Bohnenstiehl et al. (2014) and Massoth et al. (2007), respectively. Assuming a similar degree of horizontal refraction along the 9290 km long source-receiver path as between Monowai and H03S, i.e. a counterclockwise deviation of about 0.4° from 246.8°, back azimuths fall within 10 km of Pelorus, making it the most likely signal source. However, activity at an uncharted edifice between 23.5°S and Pelorus represents an equally plausible explanation for our observations, as seafloor topography in the area is poorly covered by high-resolution multibeam data and there exists a notable gap in the sequence of otherwise more or less evenly spaced volcanic edifices.

Extending the observational window south of the lower processing threshold for a source at Monowai, i.e. below the back azimuth of 238.8° as seen from the H03S array, reveals a five-day-long cluster of 2039 detections in August 2015. The cluster arrives from 234.3°, coinciding with the geodesic back azimuth to Healy, and falls within 0.3° of a source at Brothers volcano in the southern Kermadec Arc (Figure 8e-f). At peak times, activity occurs at a rate of up to 500 detections per 12 hours, with broadband, impulsive arrivals in the range of 100 to 120 dB re 1 µPa, lasting between seconds and tens of seconds (Figure 8g-h). In the

past, hydrothermal plumes were observed at both sites (de Ronde et al., 2001), and Dziak et al. (2008) report intermittent seismic activity and harmonic tremor at Brothers over the course of several months in 2005. However, it is not possible to attribute acoustic arrivals to either edifice with absolute certainty: The near-perfect match between observed and geodesic back azimuth favors a source at Healy, but considering the same angular offset derived for arrivals from Monowai (0.4°) shifts the back projected path northwards and within 15 km of Brothers volcano.

Interestingly, six earthquakes with epicenters located 50-150 km northeast of Brothers and with magnitudes of between 3.6 and 4.7 m_b were registered by the IMS network prior to the onset of activity and are amongst the first arrivals of the cluster formed by the DBSCAN algorithm. Earthquake arrivals are then followed by a two hours long period of sustained broadband tremor that precedes the beginning of the main burst by approximately 24 hours. Since tremor events can indicate resonance in a fluid-filled chamber or conduit (Chouet, 1996), often preceding or accompanying volcanic eruptions (e.g., McNutt and Nishimura, 2008), we speculate that the 2015 episode at Healy or Brothers volcano may have occurred in response to, or was aided by, dynamic stress changes induced by the nearby earthquake swarm (Walter et al., 2007). Since error ellipses are not well defined in a ridge-parallel direction (cf. Figure 8e), one could also assume that the seismic events in fact occurred much closer to, or directly at, one of the volcanoes. In this case, earthquakes could be interpreted as the result of, rather than the cause for, a submarine eruption, signaling, for example, a dyking event or the initial breaching of the magma chamber (Bohnenstiehl et al., 2013). Evidently, these interpretations only represent two of multiple possible scenarios and a more detailed analysis, which is beyond the scope of the study presented here, is needed in the future.

5. Discussion

Our observations of activity at Monowai are in good agreement with previous studies (cf. Chadwick et al., 2008a) and suggest that the 82 clusters identified by the DBSCAN algorithm indeed correspond to volcanic episodes. Even though studies of submarine volcanism remain difficult to compare due to the inherent differences of their respective surveying methods and analysis parameterization, we note that few other known sites, i.e. West Mata in the northern Tonga Arc (Bohnenstiehl et al., 2014) and NW Rota-1 in the Northern Mariana Islands (Chadwick et al., 2008b; Schnur et al., 2017), comprise an equally extensive record of unrest. At an average rate of 23 discrete episodes per year, our observations supersede previous estimates for activity at Monowai by one order of magnitude (Watts et al., 2012). These estimates were based on the growth rate of the volcano during the 5-day long eruption event in May 2011 and comparing it to the growth during 2007 and 2011 based on repeat bathymetric surveys. As Watts et al. (2012) point out, the growth rate observed during the 2011 event was unusually high compared to other submarine volcanoes (e.g. Kick ‘em Jenny in the Lesser Antilles arc) and is probably not typical of the preceding four years of activity. Irrespective, the rates of activity determined in this paper notably exceed those of other sites previously studied by the means of long-term seismoacoustic recordings, for example Macdonald Seamount and the Teahitia-Mehetia region in the South Pacific (Norris and Johnson, 1969; Talandier and Okal, 1987), making Monowai one of the most active submarine sites currently known.

At a cumulative length of 137 days of 1-min detections over the course of 3.5 years, Monowai is a major source of coherent low-frequency sound in the record of the southern hydrophone array at Juan Fernandez Islands. For instance, arrivals from the volcano amount

to 39% (196,949) of all detections at H03S (510,464), and more than 25% of the cumulative root-mean-square energy received in the 4-12 Hz band. Even though more sophisticated methods exist to distinguish in-water nuclear explosions from other seismoacoustic sources, for example by performing advanced spectral analysis (e.g., Tuma et al. 2016), activity at the volcano has to be taken into account when deriving test-ban relevant calibrations of the IMS hydrophone station at Juan Fernández Islands, e.g. during the derivation of short and long-term ocean noise levels (Brown et al., 2012). At a mean correlation coefficient of 0.61, acoustic phases from Monowai also represent an extremely coherent component of the ambient sound field at the H03S array. Future studies therefore need to assess whether persistent arrivals from the volcano can interfere with the hydroacoustic detection of earthquakes and other treaty-relevant events, both of which fall in frequency and amplitude ranges similar to those of the identified volcanic episodes (Hanson et al., 2001; Hanson and Bowman, 2005).

We find no significant relationship between local levels of seismicity and volcanism at Monowai. Over the course of the ~3.5 years long record, less than two dozen earthquakes, usually between 4 and 6.5 m_b magnitude and focal depths greater than 100 km, were detected within a 75 km radius from the volcano. None of these events occurred during or within two days prior to a volcanic episode. Bohnenstiehl et al. (2014) observe an increase in activity at numerous submarine volcanoes in the Tofua and Tonga Arc in response to two $M_w > 8.0$ earthquakes in the southern Pacific region. Comparing events of similar magnitude ($M_w \geq 7.5$) in the South Pacific region to our record of activity shows no such effect, suggesting that the volcanic regime at Monowai may be unresponsive to the static and dynamic stress changes induced by seismic activity. We note, however, that activity triggered by external

parameters, e.g. earthquakes or tidal forces, has been shown to occur at relatively low levels (Tolstoy et al., 2002) and hence, may remain undetected by the distant hydrophone array.

Previous studies report numerous, potentially active volcanic edifices in the Tonga-Kermadec Arc region (Stoffers et al., 2006; Massoth et al., 2007). Yet, only two episodes retrieved from the ~3.5 years long record of the H03S hydrophone array are not associated with activity at Monowai. The absence of further detections of active sites may be due to various reasons. For instance, shoaling bathymetry might block acoustic ray paths, as most known active submarine volcanoes along the Tonga-Kermadec Arc are located to the west of the crest of north-south trending Tonga and Kermadec ridge that reaches depths of 500 m or less (cf. Figure 8). Coupling of acoustic energy into the SOFAR domain may also be less efficient at certain sites, for example when the source is located too far below the sound channel axis (Blackman et al., 2004). Furthermore, it is possible that activity at other volcanoes is weaker, thus remaining below detectable levels, or occurs at frequencies outside the 4-12 Hz processing range used in this study.

Explosive volcanism can generate atmospheric sound waves that are frequently detected by IMS infrasound sensors (e.g., Matoza et al., 2011; 2017). Due to the high impedance contrast of the ocean-atmosphere boundary, sound emitted by a submarine volcano can become airborne only after the edifice reaches the sea surface (Green et al., 2013; Nishida and Ichihara, 2016). However, in cases where the acoustic wavelength significantly exceeds the in-water source depth (Godin, 2007), low-frequency underwater sound waves may transcend the anomalously transparent sea surface and propagate as atmospheric signals. This process is known as evanescent wave coupling and was first observed in a geophysical system by Evers et al. (2014) for the 2004 M_W 8.1 Macquarie Ridge earthquake. During times of activity at

Monowai, no corresponding arrivals are registered in the IMS processing stream at the three closest infrasound stations, i.e. IS22 at Port Laguerre (1674 km source-receiver distance), IS36 at Chatham Islands (2001 km), and IS24 at Tahiti (3014 km), suggesting that an equivalent phenomenon is not present at Monowai, and that the volcano probably failed to breach the sea surface during the time periods studied here.

6. Conclusion

We examined a 3.5-year record of hydrophone recordings at Juan Fernández Islands, Southeast Pacific Ocean, for long-range underwater sound waves from Monowai, Kermadec Arc. Our results show that the volcano was intermittently active between July 2003 and March 2004, and from April 2014 to January 2017. Density-based clustering of hydroacoustic arrivals identified 82 discrete episodes of volcanic activity during this time. Episodes occur on average twice per month, typically range from hours to multiple days in length, and amount to 137 days in total, making Monowai one of the most active sites of submarine volcanism currently known on Earth. Comparing acoustic and seismic measurements of earthquakes in the Kermadec Arc suggests a mean magnitude range of 1.6 to 3.1 m_b for detected events at the volcano. At a comparable body wave magnitude of 2.2 m_b, acoustic resolution of the H03S hydrophone array surpasses regional broadband networks by at least one order of magnitude for seismic activity at Monowai. Density-based clustering of arrivals from further persistent sources along the Tonga-Kermadec Arc revealed signs of volcanic activity at Healy or Brothers volcano in August 2015, and at a location near 23°S in the southern Tonga Arc in December 2014. Our findings are consistent with previous studies and show that remotely tracking submarine volcanic activity by the means of hydroacoustic measurements is feasible, even over basin-scale distances.

Finally, we note that the clustering algorithm applied in this study could be adapted for other array-type hydrophone deployments with relative ease, enabling the systematic scanning of waveform data for persistent sources of low-frequency ocean sound, i.e. other volcanically active sites. Our findings highlight the importance of the IMS array H03S in studying volcanism at Monowai and have implications for early warning measures: While episodes cannot be forecasted, the delay time at which ships in the area can be warned of an increase in activity at the volcano is limited only by the acoustic travel time to the H03S array and the relay time of waveform data to the International Data Centre, all in all totaling less than three hours.

Disclaimer

The views expressed in this study are those of the authors and do not necessarily reflect those of the Preparatory Commission for the CTBTO.

Acknowledgements

Hydroacoustic data were made available by the CTBTO International Data Centre, Vienna, through the virtual Data Exploitation Centre (vDEC, www.ctbto.org/specials/vdec/), and processed using MATLAB-based tools, including the Waveform Suite (*Reyes and West*, 2011). A modified version of the DBSCAN algorithm, implemented by the Yarpiz Project, was used for cluster analysis. The relevant code was obtained from the MathWorks File Exchange under "DBSCAN Clustering Algorithm". The facilities of IRIS Data Services were used for access to waveforms of the Rarotonga broadband station and earthquake metadata.

IRIS Data Services are funded through the Seismological Facilities for the Advancement of Geoscience and EarthScope (SAGE) Proposal of the National Science Foundation under Cooperative Agreement EAR-1261681. Anne Trehu (Oregon State) is much thanked for her prompt help with accessing the shot logs of the 2017 CEVICHE seismic experiment. Bill Chadwick (Oregon State/CIMRS), Olivier Hyvernaud, and Dominique Reymond (both Laboratoire de Géophysique Tahiti) provided the T phase record of station TVO of the Polynesian Seismic Network. Albert Brouwer and Ronan Le Bras (both CTBTO) advised on IMS instrumentation and database access. The authors further thank Rachel Kan (University of Essex), Maria Tsekhmistrenko, David M. Pyle, Karin Sigloch (all Oxford), Walter H. F. Smith (NOAA), Stefan Bredemeyer (GEOMAR), and Jelle Assink (KNMI) for comments and fruitful discussions.

References

Averbuch, G., J. D. Assink, P. S. M. Smets, and L. G. Evers (2018), Extracting low signal-to-noise ratio events with the Hough transform from sparse array data, *Geophysics 83 (3)*, WC43-WC51, doi:10.1190/GEO2017-0490.1.

Bassett, D., and A. B. Watts (2015), Gravity anomalies, crustal structure, and seismicity at subduction zones: 1. Seafloor roughness and subducting relief, *Geochem. Geophys. Geosyst.*, *16*(5), 1508–1540, doi:10.1002/2014GC005684.

Blackman, D. K., C. C. Groot-Hedlin, P. Harben, A. Sauter, and J. A. Orcutt (2004), Testing low/very low frequency acoustic sources for basin-wide propagation in the Indian Ocean, *J. Acoust. Soc. Am.*, *116*(4), 2057–2066, doi:10.1121/1.1786711.

Bohnenstiehl, D. R., C. M. Scheip, H. Matsumoto, and R. P. Dziak (2012), Acoustics variability of air gun signals recorded at intermediate ranges within the Lau Basin, *Geochem. Geophys. Geosyst.*, *13*(11), –n/a, doi:10.1029/2012GC004337.

Bohnenstiehl, D. R., R. P. Dziak, H. Matsumoto, and J. A. Conder (2014), Acoustic response of submarine volcanoes in the Tofua Arc and northern Lau Basin to two great

earthquakes, *Geophys. J. Int.*, *196*(3), 1657–1675, doi:10.1093/gji/ggt472.

Bohnenstiehl, D. R., R. P. Dziak, H. Matsumoto, and T. K. A. Lau (2013), Underwater acoustic records from the March 2009 eruption of Hunga Ha'apai-Hunga Tonga volcano in the Kingdom of Tonga, *J. Volc. Geotherm. Res.*, *249*, 12–24, doi:10.1016/j.jvolgeores.2012.08.014.

Brown, D., L. Ceranna, M. Prior, P. Mialle, and R. J. Le Bras (2012), The IDC Seismic, Hydroacoustic and Infrasound Global Low and High Noise Models, *Pure Appl. Geophys.*, *171*(3-5), 361–375, doi:10.1007/s00024-012-0573-6.

Calkins, J., C. Oppenheimer, and P. R. Kyle (2008), Ground-based thermal imaging of lava lakes at Erebus volcano, Antarctica, *J. Volc. Geotherm. Res.*, *177*(3), 695–704, doi:10.1016/j.jvolgeores.2008.02.002.

Caplan-Auerbach, J., R. P. Dziak, J. Haxel, D. R. Bohnenstiehl, and C. Garcia (2017), Explosive processes during the 2015 eruption of Axial Seamount, as recorded by seafloor hydrophones, *Geochem. Geophys. Geosyst.*, *18*(4), 1761–1774, doi:10.1002/2016GC006734.

Chadwick, W. W. J., I. C. Wright, U. Schwarz-Schampera, O. Hyvernaud, D. Reymond, and C. E. J. de Ronde (2008a), Cyclic eruptions and sector collapses at Monowai submarine volcano, Kermadec arc: 1998-2007, *Geochem. Geophys. Geosyst.*, *9*(10), –n/a, doi:10.1029/2008GC002113.

Chadwick, W. W. J., K. V. Cashman, R. W. Embley, H. Matsumoto, R. P. Dziak, C. E. J. de Ronde, T. K. A. Lau, N. D. Deardorff, and S. G. Merle (2008b), Direct video and hydrophone observations of submarine explosive eruptions at NW Rota-1 volcano, Mariana arc, *J. Geophys. Res.*, *113*(B8), doi:10.1029/2007JB005215.

Chapman, N. R., and A. Price (2011), Low frequency deep ocean ambient noise trend in the Northeast Pacific Ocean, *J. Acoust. Soc. Am.*, *129*(5), E161–E165, doi:10.1121/1.3567084.

Chouet, B. A. (1996), Long-period volcano seismicity: Its source and use in eruption forecasting, *Nature*, *380*(6572), 309–316, doi:10.1038/380309a0.

Davey, F. J. (1980), The Monowai Seamount - an Active Submarine Volcanic Center on the Tonga-Kermadec Ridge, *New Zeal. J. Geol. Geop.*, *23*(4), 533–536.

de Groot-Hedlin, C., D. K. Blackman, and C. S. Jenkins (2009), Effects of variability associated with the Antarctic circumpolar current on sound propagation in the ocean, *Geophys. J. Int.*, *176*(2), 478–490, doi:10.1111/j.1365-246X.2008.04007.x.

de Ronde, C., E. T. Baker, G. J. Massoth, J. E. Lupton, I. C. Wright, R. A. Feely, and R. R. Greene (2001), Intra-oceanic subduction-related hydrothermal venting, Kermadec volcanic arc, New Zealand, *Earth Planet Sci. Lett.*, *193*(3-4), 359–369.

Del Pezzo, E., and F. Giudicepietro (2002), Plane wave fitting method for a plane, small aperture, short period seismic array: a MATHCAD program, *Comput Geosci*, *28*(1), 59–64, doi:10.1016/S0098-3004(01)00076-0.

Dziak, R. P., and C. G. Fox (2002), Evidence of harmonic tremor from a submarine volcano detected across the Pacific Ocean basin, *J. Geophys. Res*, *107*(B5), doi:10.1029/2001JB000177.

Dziak, R. P., J. H. Haxel, H. Matsumoto, T. K. A. Lau, S. G. Merle, C. E. J. de Ronde, R. W. Embley, and D. K. Mellinger (2008), Observations of regional seismicity and local harmonic tremor at Brothers volcano, south Kermadec arc, using an ocean bottom hydrophone array, *J. Geophys. Res.*, *113*(B8), B08S04, doi:10.1029/2007JB005533.

Embley, R. W. et al. (2006), Long-term eruptive activity at a submarine arc volcano, *Nature*, *441*(7092), 494–497, doi:10.1038/nature04762.

Ester, M., H.-P. Kriegel, J. Sander, and X. Xu (1996), A Density-Based Algorithm for Discovering Clusters in Large Spatial Databases with Noise, *Proceedings of the Second International Conference on Knowledge Discovery and Data Mining KDD-*, 226–231, doi:10.1.1.121.9220.

Evers, L. G., D. N. Green, N. Y. Young, and M. Snellen (2013), Remote hydroacoustic sensing of large icebergs in the southern Indian Ocean: Implications for iceberg monitoring, *Geophys. Res. Lett.*, *40*(17), 4694-4699, doi:10.1002/grl.50914.

Evers, L. G., and M. Snellen (2015), Passive probing of the sound fixing and ranging channel

with hydro-acoustic observations from ridge earthquakes, *J. Acoust. Soc. Am.*, *137*(4), 2124–2136, doi:10.1121/1.4916267.

Evers, L. G., D. Brown, K. D. Heaney, J. D. Assink, P. S. M. Smets, and M. Snellen (2014), Evanescent wave coupling in a geophysical system: Airborne acoustic signals from the Mw 8.1 Macquarie Ridge earthquake, *Geophys. Res. Lett.*, *41*(5), 1644–1650, doi:10.1002/2013GL058801.

Ewing, M., F. Press, and J. L. Worzel (1951), Further Observations of the T-Phase, *Geol. Soc. Am. Bull.*, *62*(12), 1527–1527.

Fritz, H. M. et al. (2011), Field Survey of the 27 February 2010 Chile Tsunami, *Pure Appl. Geophys.*, *168*(11), 1989–2010, doi:10.1007/s00024-011-0283-5.

Global Volcanism Program (2017), *Report on Monowai (New Zealand)*, edited by E. Venzke.

Godin, O. A. (2007), Transmission of low-frequency sound through the water-to-air interface, *Acoustical Physics*, *53*(3), 305–312, doi:10.1134/S1063771007030074.

Graeber, F. M., and P.-F. Piserchia (2004), Zones of T-wave excitation in the NE Indian ocean mapped using variations in backazimuth over time obtained from multi-channel correlation of IMS hydrophone triplet data, *Geophys. J. Int.*, *158*(1), 239–256, doi:10.1111/j.1365-246X.2004.02301.x.

Green, D. N., L. G. Evers, D. Fee, R. S. Matoza, M. Snellen, P. Smets, and D. Simons (2013), Hydroacoustic, infrasonic and seismic monitoring of the submarine eruptive activity and sub-aerial plume generation at South Sarigan, May 2010, *J. Volc. Geotherm. Res.*, *257*, 31–43, doi:10.1016/j.jvolgeores.2013.03.006.

Guilbert, J., J. Vergoz, E. Schisselé, A. Roueff, and Y. Cansi (2005), Use of hydroacoustic and seismic arrays to observe rupture propagation and source extent of the Mw = 9.0 Sumatra earthquake, *Geophys. Res. Lett.*, *32*(1), 15310, doi:10.1029/2005GL022966.

Hanson, J. A., and J. R. Bowman (2005), Indian Ocean ridge seismicity observed with a permanent hydroacoustic network, *Geophys. Res. Lett.*, *32*(6), doi:10.1029/2004GL021931.

Hanson, J. A., and J. R. Bowman (2006), Methods for monitoring hydroacoustic events using

direct and reflected T waves in the Indian Ocean, *J. Geophys. Res.*, *111*(B2), doi:10.1029/2004JB003609.

Hanson, J., R. Le Bras, P. Dysart, D. Brumbaugh, A. Gault, and J. Guern (2001), Operational processing of hydroacoustics at the Prototype International Data Center, *Pure Appl. Geophys.*, *158*(3), 425–456, doi:10.1007/PL00001190.

Helffrich, G., S. I. N. Heleno, B. Faria, and J. F. B. D. Fonseca (2006), Hydroacoustic detection of volcanic ocean-island earthquakes, *Geophys. J. Int.*, *167*(3), 1529–1536, doi:10.1111/j.1365-246X.2006.03228.x.

Le Bras, R. J., H. Kuzma, V. Sucic, and G. Bokelmann (2016), Observations and Bayesian location methodology of transient acoustic signals (likely blue whales) in the Indian Ocean, using a hydrophone triplet, *J. Acoust. Soc. Am.*, *139*(5), 2656–2667, doi:10.1121/1.4948758.

Li, B. (2010), Acoustic observation of ice rifting and breaking events on the Antarctic ice shelf using remote hydroacoustic listening stations, 1–240 pp.

Massey, F. J. (1951), The Kolmogorov-Smirnov Test for Goodness of Fit, *Journal of the American Statistical Association*, *46*(253), 68–78, doi:10.2307/2280095.

Massoth, G. et al. (2007), Multiple hydrothermal sources along the south Tonga arc and Valu Fa Ridge, *Geochem. Geophys. Geosyst.*, *8*(11), –n/a, doi:10.1029/2007GC001675.

Mather, T. A. et al. (2012), Halogens and trace metal emissions from the ongoing 2008 summit eruption of Kilauea volcano, Hawaii, *Geochimica Et Cosmochimica Acta*, *83*, 292–323, doi:10.1016/j.gca.2011.11.029.

Matoza, R. S. et al. (2011), Long-range acoustic observations of the Eyjafjallajökull eruption, Iceland, April-May 2010, *Geophys. Res. Lett.*, *38*(6), n/a–n/a, doi:10.1029/2011GL047019.

Matoza, R. S., D. N. Green, A. Le Pichon, P. M. Shearer, D. Fee, P. Mialle, and L. Ceranna (2017), Automated detection and cataloging of global explosive volcanism using the International Monitoring System infrasound network, *J. Geophys. Res*, *122*(4), 2946–2971, doi:10.1002/2016JB013356.

Matsumoto, H., G. Haralabus, M. Zampolli, and N. M. Oezel (2016), T-phase and tsunami pressure waveforms recorded by near-source IMS water-column hydrophone triplets during the 2015 Chile earthquake, *Geophys. Res. Lett.*, *43*(24), 12511–12519, doi:10.1002/2016GL071425.

McNutt, S. R., and T. Nishimura (2008), Volcanic tremor during eruptions: Temporal characteristics, scaling and constraints on conduit size and processes, *J. Volc. Geotherm. Res.*, *178*(1), 10–18, doi:10.1016/j.jvolgeores.2008.03.010.

Metz, D., A. B. Watts, I. Grevemeyer, M. Rodgers, and M. Paulatto (2016), Ultra-long-range hydroacoustic observations of submarine volcanic activity at Monowai, Kermadec Arc, *Geophys. Res. Lett.*, *43*(4), 1529–1536, doi:10.1002/2015GL067259.

Munk, W. H., and A. M. G. Forbes (1989), Global Ocean Warming: An Acoustic Measure? *Journal of Physical Oceanography*, *19*(11), 1765–1780, doi:10.1175/1520-0485.

Munk, W. H., W. C. O'Reilly, and J. L. Reid (1988), Australia-Bermuda Sound-Transmission Experiment (1960) Revisited, *Journal of Physical Oceanography*, *18*(12), 1876–1898, doi:10.1175/1520-0485(1988)018<1876:ABSTER>2.0.CO;2.

Nichols, S. M., and D. L. Bradley (2016), In Situ Shape Estimation of Triangular Moored Hydrophone Arrays Using Ambient Signals, *IEEE J. Oceanic Eng.*, 1–13, doi:10.1109/JOE.2016.2625378.

Nishida, K., and M. Ichihara (2016), Real-time infrasonic monitoring of the eruption at a remote island volcano using seismoacoustic cross correlation, *Geophys. J. Int.*, *204*(2), 748–752, doi:10.1093/gji/ggv478.

Norris, R. A., and R. H. Johnson (1969), Submarine volcanic eruptions recently located in the Pacific by Sofar Hydrophones, *J. Geophys. Res.*, 1–15.

O'Malley, R. T., M. J. Behrenfeld, T. K. Westberry, A. J. Milligan, D. C. Reese, and K. H. Halsey (2014), Improbability mapping: A metric for satellite-detection of submarine volcanic eruptions, *Remote Sens. Environ.*, *140*, 596–603, doi:10.1016/j.rse.2013.09.029.

Paulatto, M., A. B. Watts, and C. Peirce (2014), Potential field and high-resolution bathymetry investigation of the Monowai volcanic centre, Kermadec Arc: implications

for caldera formation and volcanic evolution, *Geophys. J. Int.*, *197*(3), 1484–1499, doi:10.1093/gji/ggt512.

Pulli, J. J., and Z. M. Upton (2002), Hydroacoustic observations of Indian earthquake provide new data on T-waves, *Eos*, *83*(13), 145–151, doi:10.1029/2002EO000090.

Reyes, C. G., and M. E. West (2011), The Waveform Suite: A Robust Platform for Manipulating Waveforms in MATLAB, *Seismol. Res. Lett.*, *82*(1), 104–110, doi:10.1785/gssrl.82.1.104.

Rolling Deck to Repository Program (2017), *Cruise MGL1701 on RV Marcus G. Langseth*, edited by N. Bangs, Rolling Deck to Repository (R2R) Program.

Schnur, S. R., W. W. Chadwick, R. W. Embley, V. L. Ferrini, C. E. J. de Ronde et al. (2017), A decade of volcanic construction and destruction at the summit of NW Rota-1 seamount: 2004-2014, *J. Geophys. Res*, *122*(3), 1558–1584, doi:10.1002/2016JB013742.

Schwarz-Schampera, U., R. Botz, M. Hannington et al. (2007), RV SONNE - Cruise report SO192-2 MANGO, GEOMAR Helmholtz Center for Ocean Research Kiel, Kiel

Sirovic, A., S. M. Wiggins, and E. M. Oleson (2013), Ocean noise in the tropical and subtropical Pacific Ocean, *J. Acoust. Soc. Am.*, *134*(4), 2681–2689, doi:10.1121/1.4820884.

Smith, D. K., M. Tolstoy, C. G. Fox, D. R. Bohnenstiehl, H. Matsumoto, and M. J. Fowler (2002), Hydroacoustic monitoring of seismicity at the slow-spreading Mid-Atlantic Ridge, *Geophys. Res. Lett.*, *29*(1), 1518, doi:10.1029/2001GL013912.

Stevens, J. L., G. E. Baker, R. W. Cook, G. L. D'Spain, Berger, L. P., and S. M. Day (2001), Empirical and Numerical Modeling of T-phase Propagation from Ocean to Land, *Pure Appl. Geophys.*, *158*(3), 531–565, doi:10.1007/PL00001194.

Stoffers, P. et al. (2006), Submarine volcanoes and high-temperature hydrothermal venting on the Tonga arc, southwest Pacific, *Geology*, *34*(6), 453–456, doi:10.1130/G22227.1.

Talandier, J., and E. A. Okal (1987), Seismic Detection of Underwater Volcanism - the Example of French Polynesia, *Pure Appl. Geophys.*, *125*(6), 919–950, doi:10.1007/BF00879361.

Talandier, J., and G. T. Kuster (1976), Seismicity and Submarine Volcanic Activity in French Polynesia, *J. Geophys. Res.*, *81*(5), 936–948, doi:10.1029/JB081i005p00936.

Talandier, J., O. Hyvernaud, D. Reymond, and E. A. Okal (2006), Hydroacoustic signals generated by parked and drifting icebergs in the Southern Indian and Pacific Oceans, *Geophys. J. Int.*, *165*(3), 817–834, doi:10.1111/j.1365-246X.2006.02911.x.

Tuma, M., V. Rorbech, M. K. Prior, and C. Igel (2016), Integrated Optimization of Long-Range Underwater Signal Detection, Feature Extraction, and Classification for Nuclear Treaty Monitoring, *IEEE Trans. Geosci. Remote Sens. Lett.*, 54(6), 3649-3659.

Tolstoy, I., M. Ewing, and F. Press (1949), T Phase of Shallow-Focus Submarine Earthquakes, *Geol. Soc. Am. Bull.*, *60*(12), 1957–1957.

Tolstoy, M., and D. R. Bohnenstiehl (2005), Hydroacoustic constraints on the rupture duration, length, and speed of the Great Sumatra-Andaman Earthquake, *Seismol. Res. Lett.*, *76*(4), 419–425.

Tolstoy, M., F. L. Vernon, J. A. Orcutt, and F. K. Wyatt (2002), Breathing of the seafloor: Tidal correlations of seismicity at Axial volcano, *Geology*, *30*(6), 503–506, doi:10.1130/0091-7613(2002)030<0503:BOTSTC>2.0.CO;2.

Walter, T. R., R. Wang, M. Zimmer, H. Grosser, B. Lühr, and A. Ratdomopurbo (2007), Volcanic activity influenced by tectonic earthquakes: Static and dynamic stress triggering at Mt. Merapi, *Geophys. Res. Lett.*, *34*(5), L05304, doi:10.1029/2006GL028710.

Ward, R., A. N. Gavrilov, and R. D. McCauley (2017), "Spot" call: A common sound from an unidentified great whale in Australian temperate waters, *J. Acoust. Soc. Am.*, *142*(2), EL231–EL236, doi:10.1121/1.4998608.

Watts, A. B., C. Peirce, I. Grevemeyer, M. Paulatto, W. Stratford, D. Bassett, J. A. Hunter, L. M. Kalnins, and C. E. J. de Ronde (2012), Rapid rates of growth and collapse of Monowai submarine volcano in the Kermadec Arc, *Nature Geosci.*, *5*(7), 510–515, doi:10.1038/ngeo1473.

Werner, R., D. Nürnberg, and F. Hauff (2013), *RV SONNE - Cruise Report SO225*, Kiel.

Wiemer, S., and M. Wyss (2000), Minimum magnitude of completeness in earthquake

catalogs: Examples from Alaska, the western United States, and Japan, *B. Seismol. Soc. Am.*, *90*(4), 859–869, doi:10.1785/0119990114.

Woessner, J., and S. Wiemer (2005), Assessing the Quality of Earthquake Catalogues: Estimating the Magnitude of Completeness and Its Uncertainty, *B. Seismol. Soc. Am.*, *95*(2), 684–698, doi:10.1785/0120040007.

Wormald, S. C., I. C. Wright, J. M. Bull, G. Lamarche, and D. J. Sanderson (2012), Morphometric analysis of the submarine arc volcano Monowai (Tofua-Kermadec Arc) to decipher tectono-magmatic interactions, *J. Volc. Geotherm. Res.*, *239*, 69–82, doi:10.1016/j.jvolgeores.2012.06.004.

Wright, I. C., W. W. J. Chadwick, C. E. J. de Ronde, D. Reymond, O. Hyvernaud, H.-H. Gennerich, P. Stoffers, K. Mackay, M. A. Dunkin, and S. C. Bannister (2008), Collapse and reconstruction of Monowai submarine volcano, Kermadec arc, 1998-2004, *J. Geophys. Res.*, *113*(B8), doi:10.1029/2007JB005138.

Wyss, M., R. E. Habermann, and J. C. Griesser (1984), Seismic Quiescence and Asperities in the Tonga-Kermadec Arc, *J. Geophys. Res.*, *89*(NB11), 9293–9304, doi:10.1029/JB089iB11p09293.

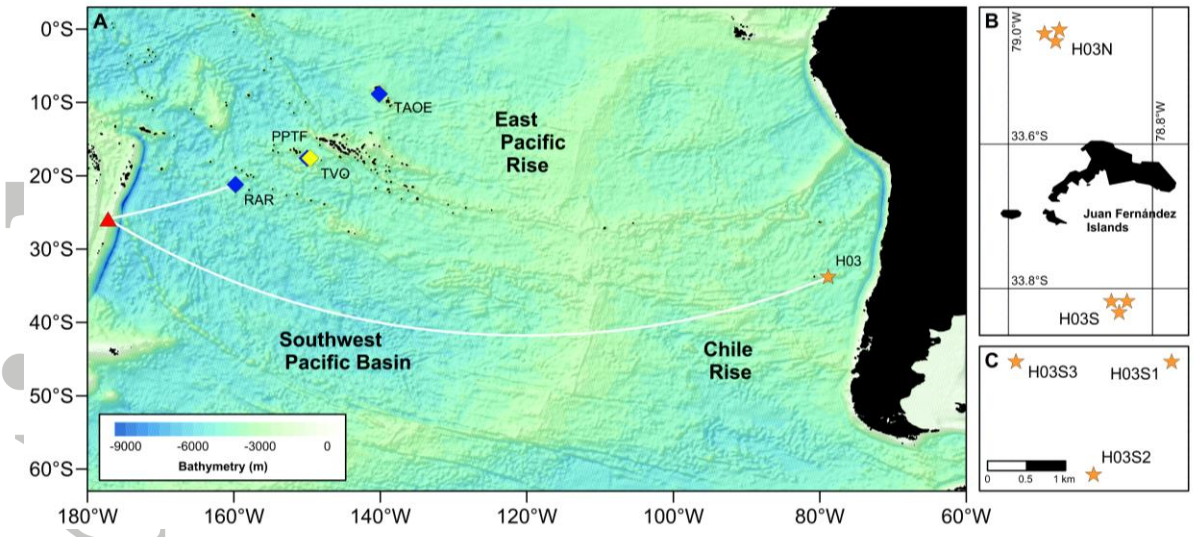

Figure 1: (a) Overview map of the Monowai Volcanic Centre (red triangle), IMS station H03 (orange star) and the three broadband seismic stations (blue diamonds) at Rarotonga (RAR), Tahiti (PPTF), and Marquesas Islands (TAOE). The stations are located at 1847 km, 2991 km, and 4340 km respectively from the volcano. Taravao station (TVO) of the Polynesian Seismic Network (yellow diamond) is also located at Tahiti. The white lines mark the two main source-receiver paths referred to in the methodology of this study (Sections 2 and 3). (b) Position map of the two hydrophone arrays at Juan Fernández Islands, moored approximately 15 km offshore to the north (H03N) and south (H03S). (c) Configuration of the southern H03 hydrophone array. The geodesic distance between Monowai and the triplet is 9165 km.

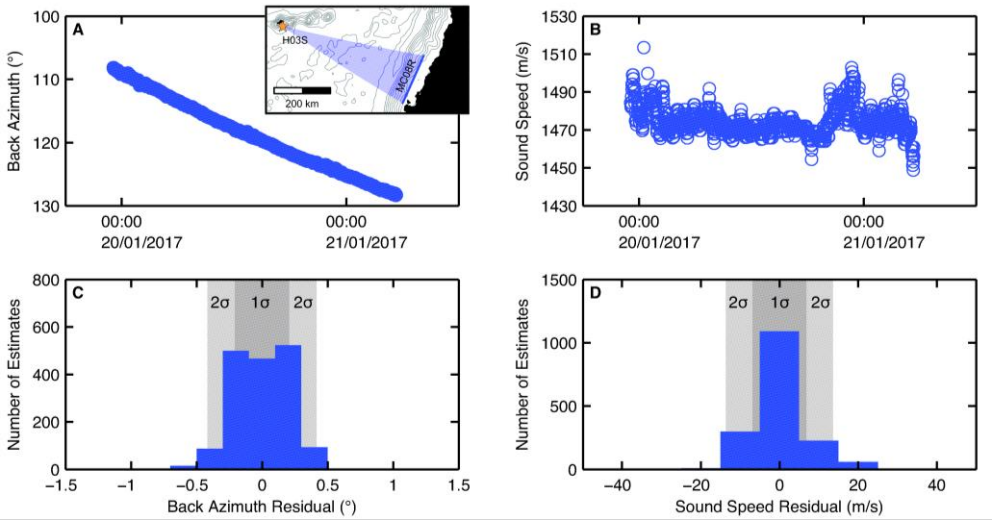

Figure 2: Uncertainty analysis of back azimuths calculated from H03S hydrophone triplet data. (a-b) Back azimuth and sound speed of 1689 1-min detections (blue circles) of 4013 air gun shots generated along a seismic reflection profile of the CEVICHE experiment between 23:00 UTC 19 and 05:00 UTC 21 January 2017. The inset shows the location of the seismic sources along profile MC08R between 109 and 130° back azimuth (dark blue line and shaded area), as seen from the southern H03 array (orange star). The survey is carried out at a southwestern heading and at an average distance of 567 ± 7 km from H03S, with start and end coordinates of the included shots at 35.36°S, 73.00°W and 37.07°S, 73.77°W. Grey bathymetric contour lines are spaced at 500 m intervals. (c) Distribution of residuals between observed and geodesic back azimuth of the detections shown in Figure 2a. Dark and light grey shaded areas mark one and two sigma standard deviations at 0.2 and 0.4°, respectively. A systematic error of -1.3 ± 0.2° is omitted for clarity. (d) Distribution of residuals between observed and nominal sound speed across the array. The detections shown in Figure 2b average at 1474 ± 7 m/s, at an offset of 7 m/s from the value indicated by the 2005 World Ocean Atlas (1481 m/s). One and two standard deviation uncertainties are at 7 and 14 m/s respectively.

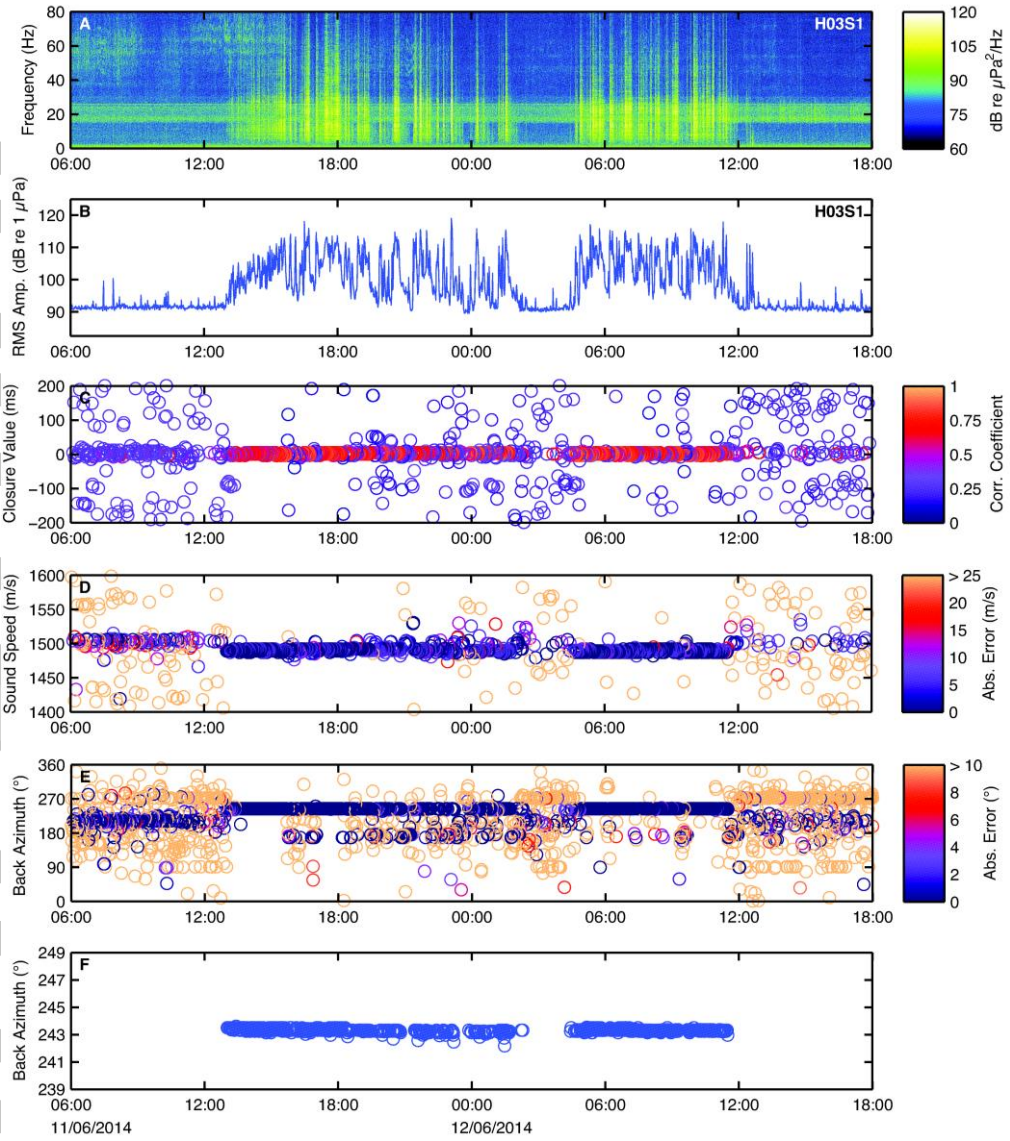

Figure 3: 36 hours of hydroacoustic data recorded at station H03S, beginning at 06:00 UTC 11 June 2014. Supporting Figure S2 shows the corresponding 36 hours of data recorded at the northern triplet array. (a) Single-receiver spectrogram of the H03S1 hydrophone data. A 2 Hz high-pass filter is applied to minimize background noise; however, wide-band contamination is present between 18 and 26 Hz, most likely due to whale calls. Note that the high-pass filter of 2 Hz, chosen to visualize the dynamic range of the hydrophone recordings, differs from the 4-12 Hz processing band. (b) Root-mean-square (RMS) amplitudes calculated over 1-min windows in the 4-12 Hz band. Processing parameters and results of the plane wave fitting routine are shown in the form of (c) closure function of summed lag times and mean correlation coefficient between hydrophone pairs, (d) apparent sound speed across the array, and (e) back azimuth. Arrivals from Monowai are recognizable in all subfigures: Hydroacoustic phases, most distinguishable between 2 and 20 Hz, arrive from 13:00 UTC onward, accompanied by a positive shift in RMS amplitude of up to 25 dB re 1 µPa above the noise floor. Coherent phases clearly stabilize at a sound speed of 1480-1485 m/s and back azimuth of ~243.4°, indicating a continuous signal that travels in the deep sound channel and that is within 0.4° of the geodesic angle of arrival for a source at the volcano (243.8°). (f) shows 1-min detections after filtering the data using the previously defined thresholds of $cc >$ 0.3, $cl < |48|$ ms, and a sound speed range of 1431-1531 m/s.

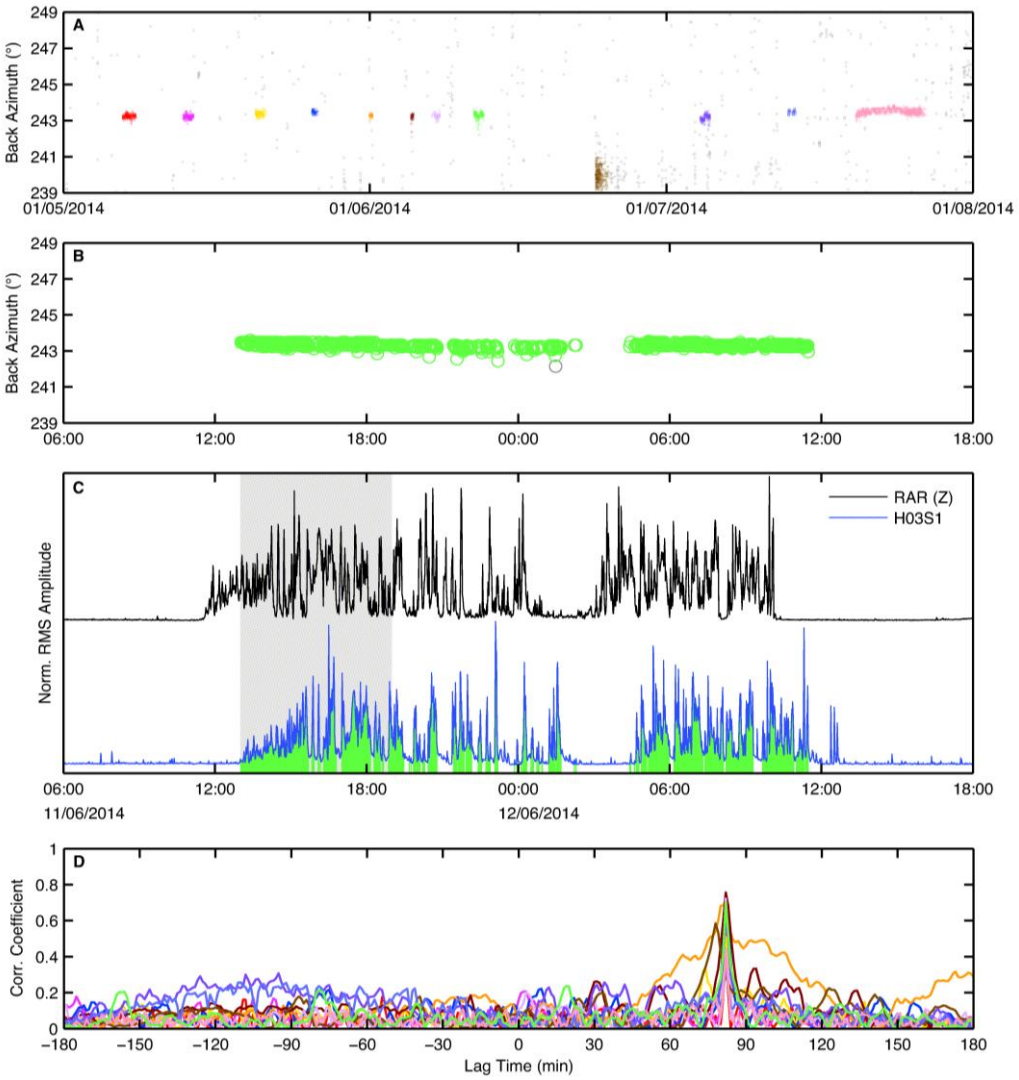

Figure 4: Density-based clustering and signal cross-correlation. (a) Results of the DBSCAN algorithm for a three-month period, beginning at 00:00 UTC 1 May 2014. Colored circles mark 1-min detections assigned to a cluster by the DBSCAN algorithm, using a minimum number of m = 60 and a search radius ε of 0.5° on the y-axis and 12h on the x-axis. Grey circles are noise. (b) Back azimuths of clustered detections between 06:00 UTC 11 June 2014 and 18:00 UTC 12 June 2014. Data corresponds to the green cluster in Figure 4a and the volcanic episode shown in Figure 3. (c) Normalized RMS amplitudes at the RAR broadband station (vertical component) and the H03S1 hydrophone, calculated over 1-min windows. The data are band-pass filtered at 2-6 Hz and 4-12 Hz, respectively. Green stems correspond to 1-min detections associated with the cluster shown in Figure 4b. The grey shaded area represents the six-hour period with the highest density of detections and delimits the segments of the RMS envelopes used in the cross-correlation. (d) Cross-correlation results of clusters shown in Figure 4a (matching colors). The distinct peaks of the correlation coefficients indicate lag times of 82 min, suggesting that the signals arrive 1 h and 22 min earlier at the Rarotonga seismometer relative to the H03S1 hydrophone at Juan Fernández Islands, which matches a source location at Monowai. The brown line indicates the lag time of detections associated with a 6.9 m_b magnitude earthquake in the central Kermadec Arc

(brown cluster in Figure 4a). Since the cluster fails to match the designated lag of 82 min, it is not added to the long-term record of volcanic episodes at Monowai.

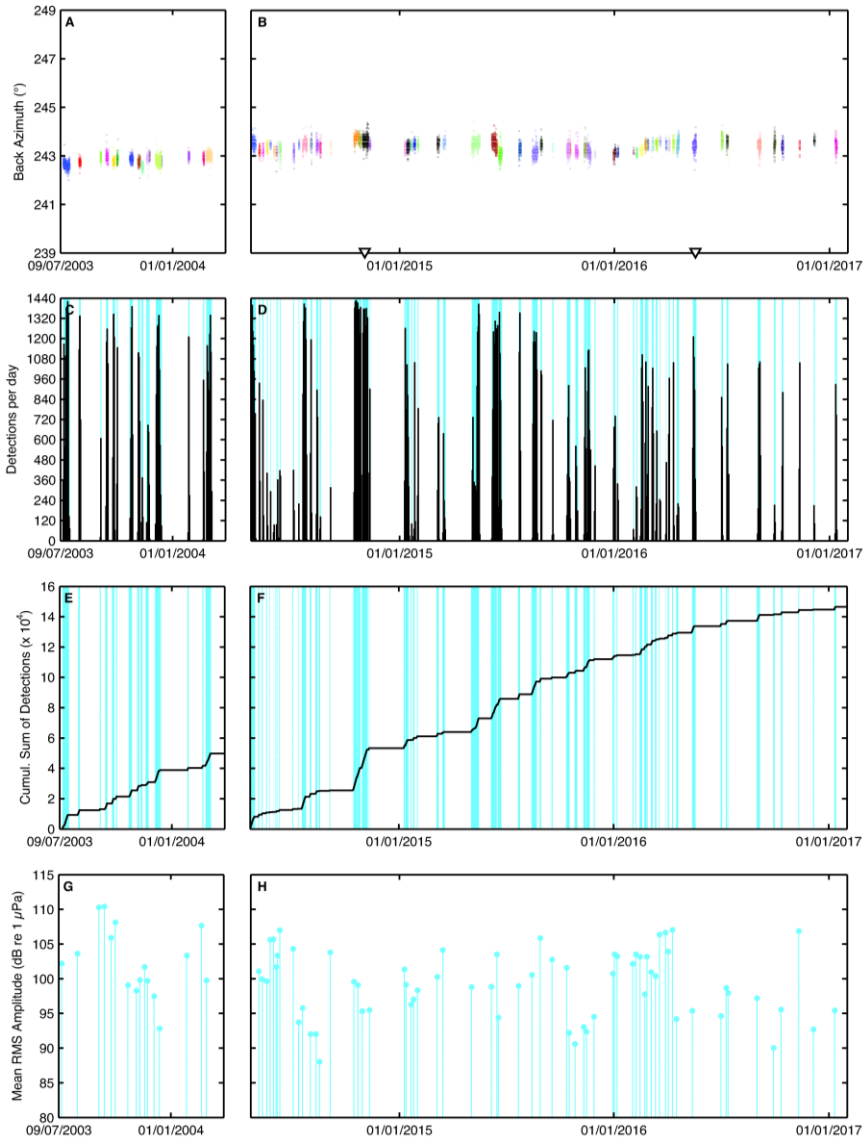

Figure 5: Record of volcanic activity at Monowai, 10 July 2003 to 25 March 2004 (left column), and 23 April 2014 to 31 January 2017 (right column). (a-b) Clustering results of hydroacoustic detections at H03S arriving from within 5° of the geodesic back azimuth to Monowai, i.e. from 238.8° to 248.8°. 82 clusters (different colors) were identified in the record, comprising a total of 196,949 1-min detections. Note that derived back azimuths vary slightly between the 2003-04 and 2014-17 period due to the different positions of H03S hydrophone elements before and after their reinstallation in 2014. White triangles mark observations of floating debris and discolored water on 31 October 2014 and 19 May 2016, respectively (Global Volcanism Program, 2017). (c-d) Number of 1-min detections per calendar day. Blue shaded areas correspond to clusters shown in Figure 5a-b. (e-f) Cumulative sum of detections, calculated separately for both periods. 49,838 detections are made from July 2003 to March 2004, and 147,111 between April 2014 and January 2017. (g-h) Mean RMS amplitudes of the identified clusters, calculated from 1-min windows in the 4-12 Hz band.

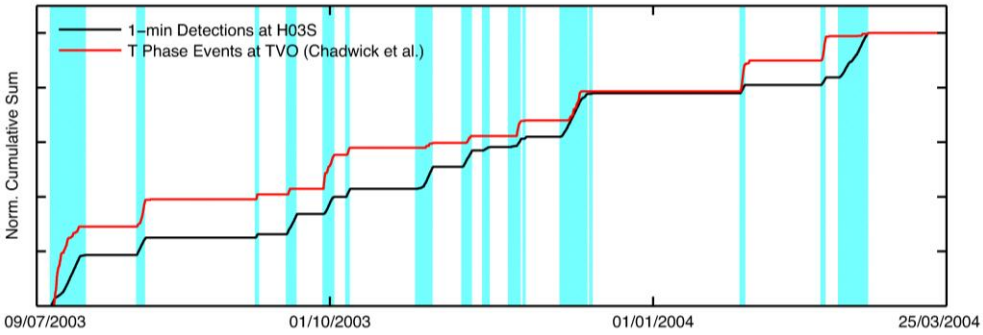

Figure 6: Comparison of the normalized cumulative number of 1-min detections at the southern H03 array (black line) with T phase events registered at TVO station of the Polynesian Seismic Network (red line) between July 2003 and March 2004 (Chadwick et al., 2008a). 854 of the 869 T phase events fall within the bounds of one of the 16 episodes of activity as defined in this study (blue shaded areas, see also Figure 5e). The black and red lines are highly similar at a cross-correlation coefficient of 0.98.

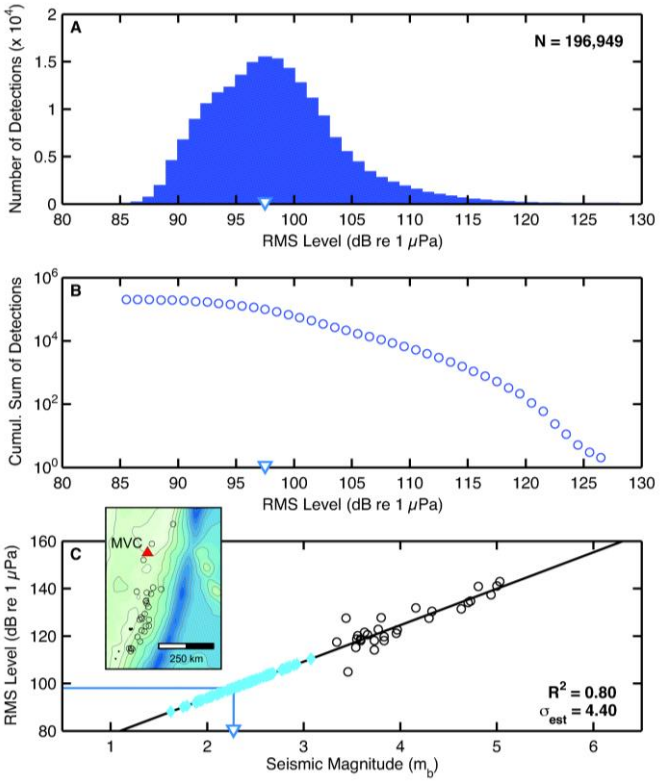

Figure 7: Resolution and seismic magnitude. (a) RMS amplitude distribution of all 196,949 1-min detections recorded at IMS hydrophone H03S1 binned to 1 dB intervals. The blue and white filled triangle marks the level of acoustic resolution at 97 dB re 1 µPa, calculated according to Wiemer and Wyss (2000). (b) Cumulative frequency-magnitude distribution of 1-min detections shown in Figure 7a. Note the logarithmic scaling of the y-axis. (c) RMS pressure amplitude of 28 earthquakes (black circles) registered by the IMS seismic network and hydrophone H03S1. Events are located between 25 and 30°S along the Kermadec Arc (see inset), at source-receiver distances of 8950 to 9175 km and focal depths of up to 80 km. The black line marks the least-square fit of the regression, which is significant at $R^2 = 0.80$ and an error of 4.40 dB re 1 µPa. Following the derived trend, acoustic resolution of 97 dB re 1 µPa corresponds to a body wave magnitude of 2.2 m_b at Monowai (blue line and triangle). Mean RMS amplitudes of the 82 episodes range from 88 to 110 dB re 1 µPa (light blue diamonds), suggesting comparable mean magnitudes between 1.6 and 3.1 m_b. Acoustic

amplitudes of individual arrivals translate into a seismic magnitude range of 1.4 to 4.2 m_b, with less than 1000 events greater than 3.5 m_b.

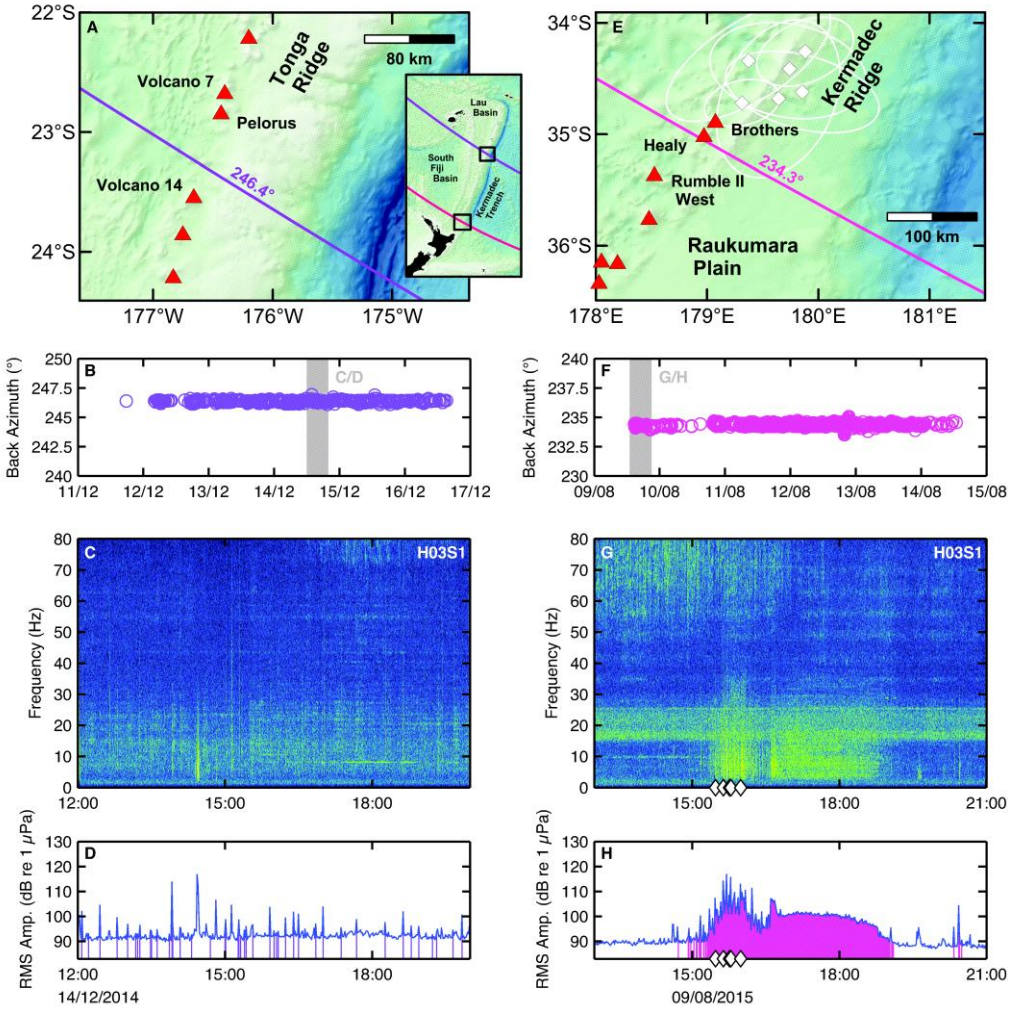

Figure 8: Observations of two presumed episodes of volcanic activity in the Tonga-Kermadec Arc. Note that in accordance with their appearance in the text, subfigures follow a column-wise order, but are captioned row by row. (Row 1: a,e) Back projection of mean azimuths (colored lines) of clustered 1-min detections across the southern Tonga and Kermadec Arc (see inset of Subfigure 8a for map locations). White diamonds in Subfigure 8e mark the epicenters and respective error ellipses of six seismic events registered by the IMS network northeast of the Healy and Brothers domain at the beginning of the cluster. (Row 2: b,f) Back azimuths of detections over the course of the two episodes. Grey shaded areas mark the positions of the spectrogram and RMS data shown in the following subfigures. (Row 3: c,g) 8-Hour single receiver spectrograms of hydrophone data recorded at H03S1, beginning at 12:00 UTC 14 December 2014 and 13:00 UTC 09 August 2015, respectively. In Subfigure 8g, background noise due to whale vocalization is present in the 16-26 Hz band, partially overlapping with the acoustic arrivals of earthquakes shown in 8e (white diamonds), and the distinct tremor signal between 16:30 and 19:00 UTC. (Row 4: d,h) 1-min RMS amplitudes during the 8-hour time windows. Colored stems indicate times of detections at the H03S

array. White diamonds correspond to hydroacoustic arrivals of earthquakes shown in Subfigure 8e.